

## Supplementary Information

### **Heterostructure of [CoAlO/Ni]@C constructed based on interface and component coupling effect toward microwave absorption and thermal conductivity**

Xiao Li <sup>a,b</sup>, Yong Zhang\* <sup>a,b</sup>, Jiale Cheng <sup>a,b</sup>, Zhongxin Huang <sup>a,b</sup>, Jiewu Cui <sup>a,b</sup>, Jiaheng Wang <sup>a,b</sup>, Yunfei Wu <sup>a,b</sup>, Yan Wang <sup>a,b</sup>, Jiaqin Liu <sup>b,c</sup>, Yucheng Wu\* <sup>a,b</sup>

*a. School of Materials Science and Engineering, Hefei University of Technology, Hefei 230009, Anhui, China.*

*b. Key Laboratory of Advanced Functional Materials and Devices of Anhui Province, Hefei 230009, China*

*c. Institute of Industry & Equipment Technology, Hefei University of Technology, Hefei 230009, Anhui, China*

Email address: zhangyong.mse@hfut.edu.cn (Yong Zhang), ycwu@hfut.edu.cn (Yucheng Wu)

## Characterizations and measurements

The microstructures of the samples were observed via scanning electron microscope (SEM) (Regulus 8230, Hitachi, Japan) as well as transmission electron microscope (TEM) (JEM-2100F, Electronics Corporation of Japan). The functional groups information of were tested by the infrared spectrometer (FTIR) (Nicolet iS50R, Thermo Fisher, USA). The phase details of the specimens were detected by X-ray diffraction (XRD) with Cu K $\alpha$  radiation (PANalytical X-Pert PRO MPD, Netherlands). The surface chemical states of the samples were explored by X-ray photoelectron spectrometer (XPS) (ESCALAB 250Xi, Thermo Fisher, USA). The Raman spectra of the final products were obtained through the inVia Raman microscope (HORIBA, LabRam HR Evolution) under 532 nm argon ion laser from 500 to 2500 cm<sup>-1</sup>. The pore size and surface area of samples were tested using surface area and porosity analyzer (Autosorb-IQ3). Thermogravimetric analysis (TG, PE, TGA-8000) was tested by heating the sample at 10°C/min under the N<sub>2</sub> atmosphere. The samples were made into 0.1 mm films and the conductivity was tested using the four-probe station (Rooko, FT-340). The samples were mixed with PVDF and pressed into a 10 mm × 10 mm cube, and then the thermal conductivity was measured through a laser thermal conductivity instrument (NETZSCH LFA457).

## Microwave absorption performance measurements

The samples were mixed with polyvinylidene fluoride (PVDF) and pressed into a concentric ring ( $\varphi_{\text{out}} = 3.04$  mm,  $\varphi_{\text{in}} = 7.00$  mm), which was then tested using the vector network analyzer (VAN, Rohde & Schwarz, ZNA43) according to the coaxial manner. And the RL figures were calculated applying the following formulas [1]:

$$\text{RL} = 20 \lg \left| \frac{Z_{\text{in}} - Z_0}{Z_{\text{in}} + Z_0} \right| \quad (\text{S1})$$

$$Z_{\text{in}} = Z_0 \sqrt{\frac{\mu_r}{\varepsilon_r} \tanh \left[ j \left( \frac{2\pi f d}{c} \right) \sqrt{\mu_r \varepsilon_r} \right]} \quad (\text{S2})$$

As shown above,  $Z_{\text{in}}$  stands for the input impedance of samples and  $Z_0$  is the impedance of air.  $\varepsilon_r$  and  $\mu_r$  represent relative complex permittivity ( $\varepsilon_r = \varepsilon' + j\varepsilon''$ ) and

relative complex permeability ( $\mu_r = \mu' + j\mu''$ ), respectively. And  $f$  and  $c$  are the frequency and velocity of EMW. As for  $d$ , it denotes the thickness of the sample.

The  $C_0$  curve for explaining magnetic loss types was calculated according to the following formula [2]:

$$C_0 = \frac{\mu''}{(\mu')^2 f} \quad (S3)$$

The attenuation constant ( $\alpha$ ) of samples was calculated through the following formula [3]:

$$\alpha = \frac{\sqrt{2}\pi f}{c} \sqrt{(\varepsilon''\mu'' - \varepsilon'\mu') + \sqrt{(\varepsilon''\mu'' - \varepsilon'\mu')^2 + (\varepsilon''\mu'' + \varepsilon'\mu')^2}} \quad (S4)$$

The impedance matching can be represented by the delta ( $\Delta$ ) [4]:

$$|\Delta| = |\sinh^2(Kfd) - M| \quad (S5)$$

$$K = \frac{4\pi\sqrt{\varepsilon'\mu'} \times \sin\left(\frac{\delta_\varepsilon + \delta_\mu}{2}\right)}{c \times \cos \delta_\varepsilon \times \cos \delta_\mu} \quad (S6)$$

$$M = \frac{4\mu'\cos \delta_\varepsilon \times \varepsilon'\cos \delta_\mu}{(\mu'\cos \delta_\varepsilon - \varepsilon'\cos \delta_\mu)^2 + \left[\tan\left(\frac{\delta_\varepsilon - \delta_\mu}{2}\right)\right]^2 \times (\mu'\cos \delta_\varepsilon - \varepsilon'\cos \delta_\mu)^2} \quad (S7)$$

According to Debye relaxation theory, dielectric loss can be divided into conduction loss ( $\varepsilon_c''$ ) and polarization loss ( $\varepsilon_p''$ ) by introducing conductivity ( $\sigma$ ) into complex dielectric constant [5]:

$$\varepsilon'' = \varepsilon_p'' + \varepsilon_c'' = \frac{2\pi f\tau(\varepsilon_s - \varepsilon_\infty)}{1 + (2\pi f)^2\tau^2} + \frac{\sigma}{2\pi f\varepsilon_0} \quad (S8)$$

The  $\varepsilon_\infty$  represents the relative dielectric constant at high-frequency limit,  $\varepsilon_0$  is the vacuum dielectric constant ( $8.85 \times 10^{-12}$  F/m),  $\tau$  is relaxation time, and  $\varepsilon_s$  represents the static dielectric constant.

The quarter wavelength model could be described as following [6]:

$$t_m = \frac{n\lambda}{4} = \frac{nc}{4f_m\sqrt{|\varepsilon_r\mu_r|}} \quad (n = 1, 3, 5 \dots) \quad (S9)$$

Where  $t_m$  and  $f_m$  are the thickness of absorbing material and the frequency corresponding to the RL peak,  $\lambda$  is the wavelength of EMW, and  $c$  is the speed of light.

### **CS simulations**

CST STUDIO SUITE 2022 was utilized to demonstrate the radar cross-section (RCS) response of CNC specimens to microwaves under far-field conditions at 15.56 GHz. Specifically, the CNC was covered on the 200 mm  $\times$  200 mm  $\times$  5 mm perfect electrical conductor (PEC) plate, and the thickness was set to 1.81 mm as the wave absorbing layer. The linear plane wave entered in the opposite direction along z-axis and varied from  $-90^\circ$  to  $90^\circ$  in the X-O-Z plane. The RCS values of the samples can be described as follows [7]:

$$\sigma \text{ (dBm}^2\text{)} = 10\log\left(\frac{4\pi S |E_s|}{\lambda^2 |E_i|}\right)^2 \quad (\text{S10})$$

Among them,  $S$  is the area of the simulation model,  $\lambda$  is the wavelength of the EMW,  $E_s$  and  $E_i$  are the electric field strengths of the scattered wave and the incident wave.

## Supplementary Figures

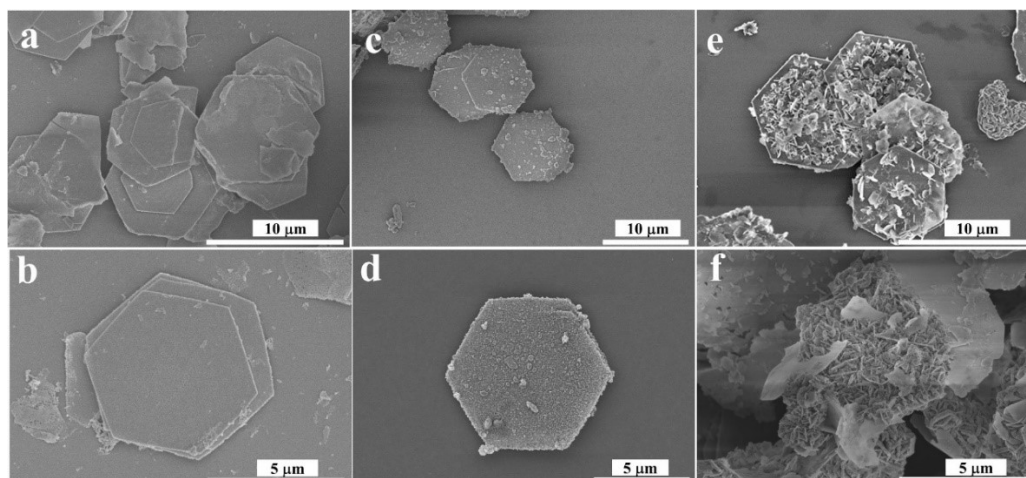


**Fig. S1.** SEM images of (a) CoAl-LDHs, (b) CoAlO, (c) CoAl-LDHs@PDA-1, (d) CoAlO@C-1, (e) CoAl-LDHs/Ni(OH)<sub>2</sub>, (f) CoAlO/NiO.

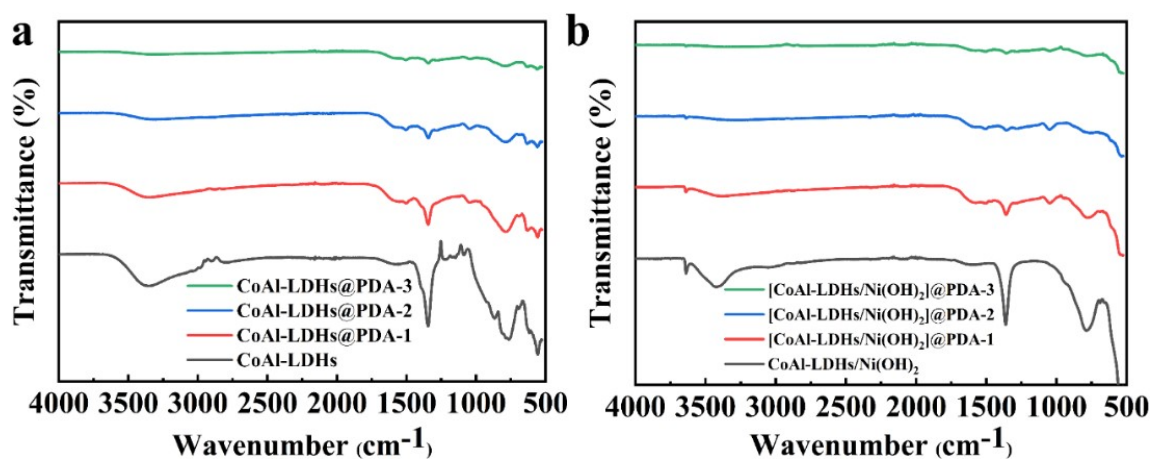


**Fig. S2.** (a) FT-IR spectra of CoAl-LDHs and CoAl-LDHs@PDA, (b) CoAl-LDHs/Ni(OH)<sub>2</sub> and [CoAl-LDHs/Ni(OH)<sub>2</sub>]@PDA.

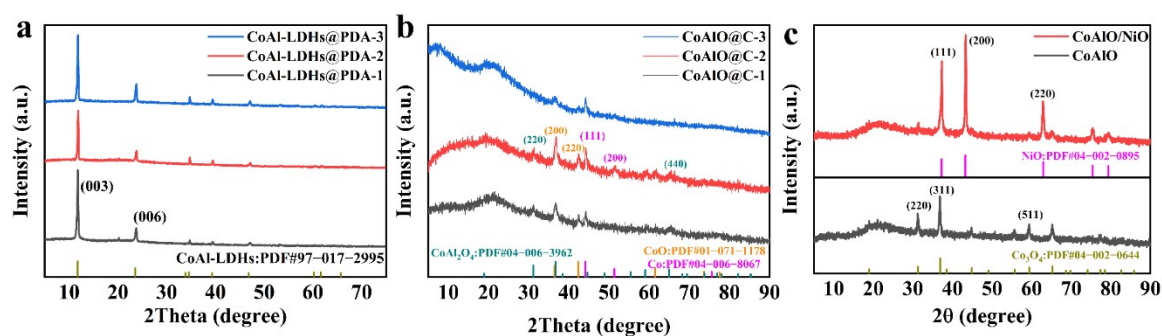


**Fig. S3.** XRD images of (a) CoAl-LDHs@PDA, (b) CoAlO@C, (c) CoAlO and CoAlO/NiO.

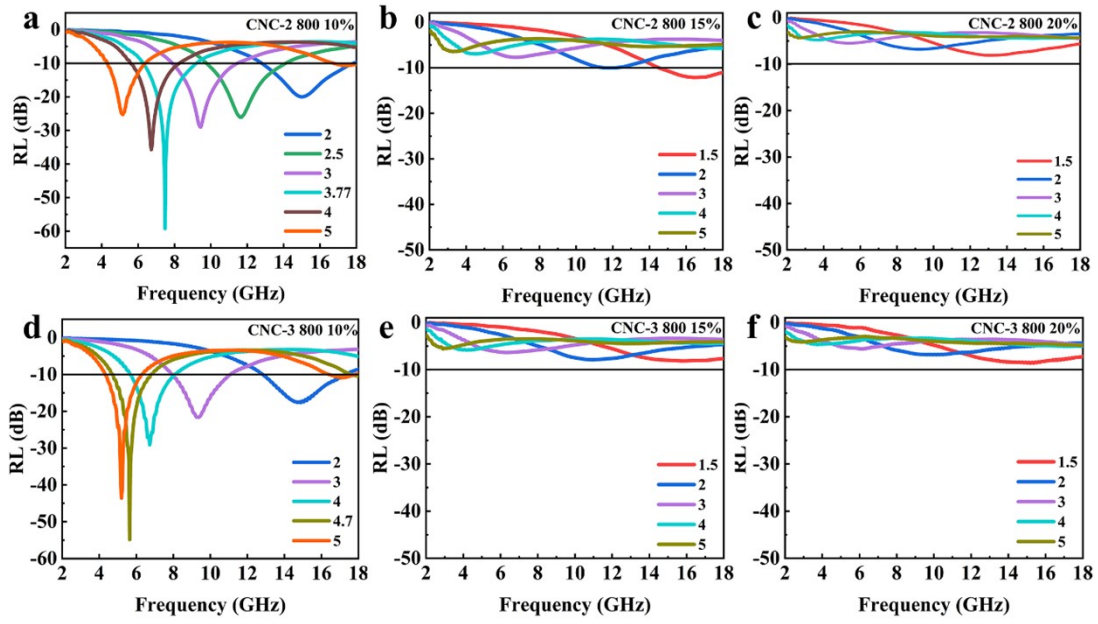


**Fig. S4.** The RL curves of (a-c) CNC-2, (d-f) CNC-3 with different filler loading.

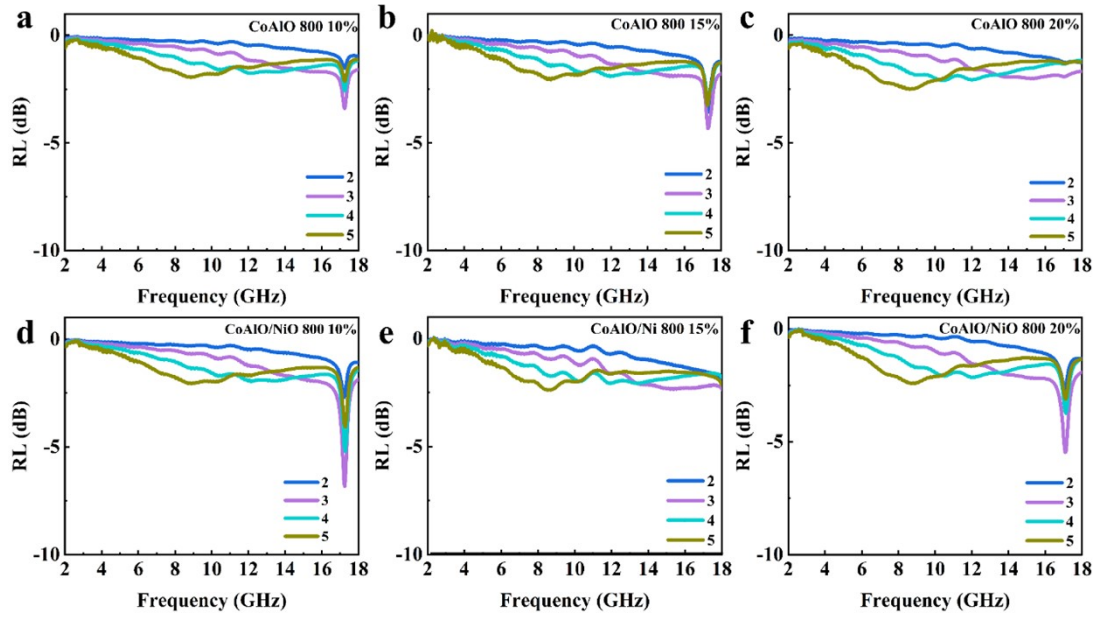


**Fig. S5.** The RL curves of (a-c) CoAlO, (d-f) CoAlO/NiO with different filler loading.

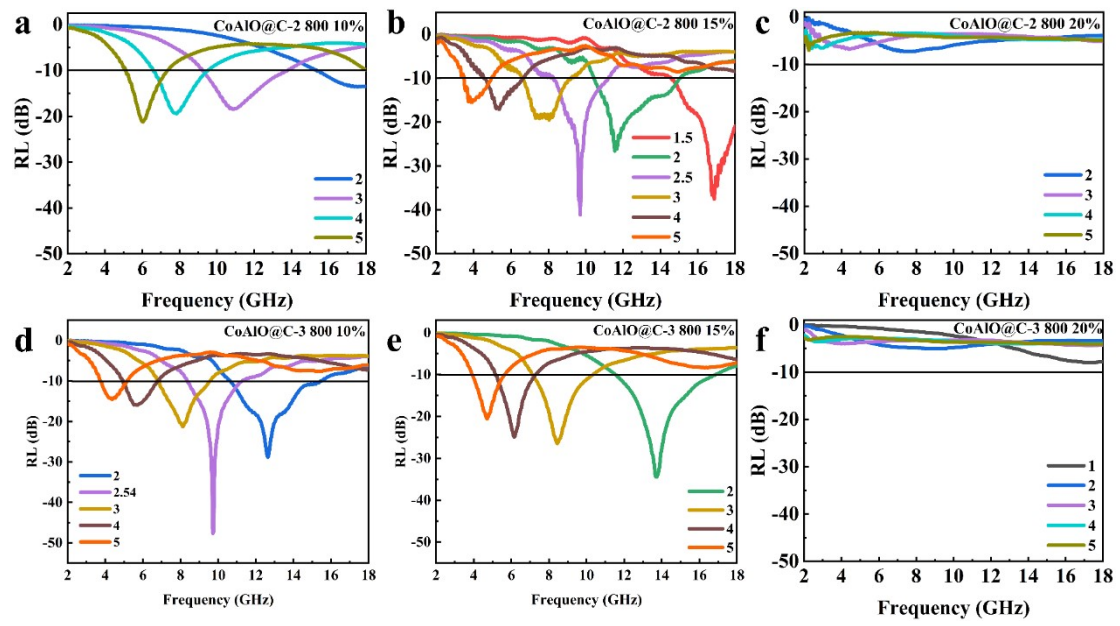


**Fig. S6.** The RL curves of (a-c) CoAlO@C-2, (d-f) CoAlO@C-3 with different filler loading in 2-18 GHz.

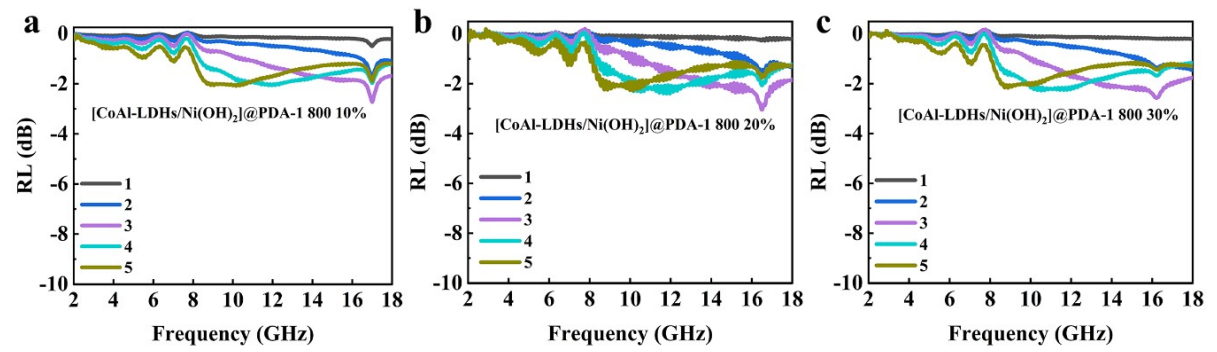


**Fig. S7.** The RL curves of (a-c) [CoAl-LDHs/Ni(OH)<sub>2</sub>]@PDA with different filler loading in 2-18 GHz.

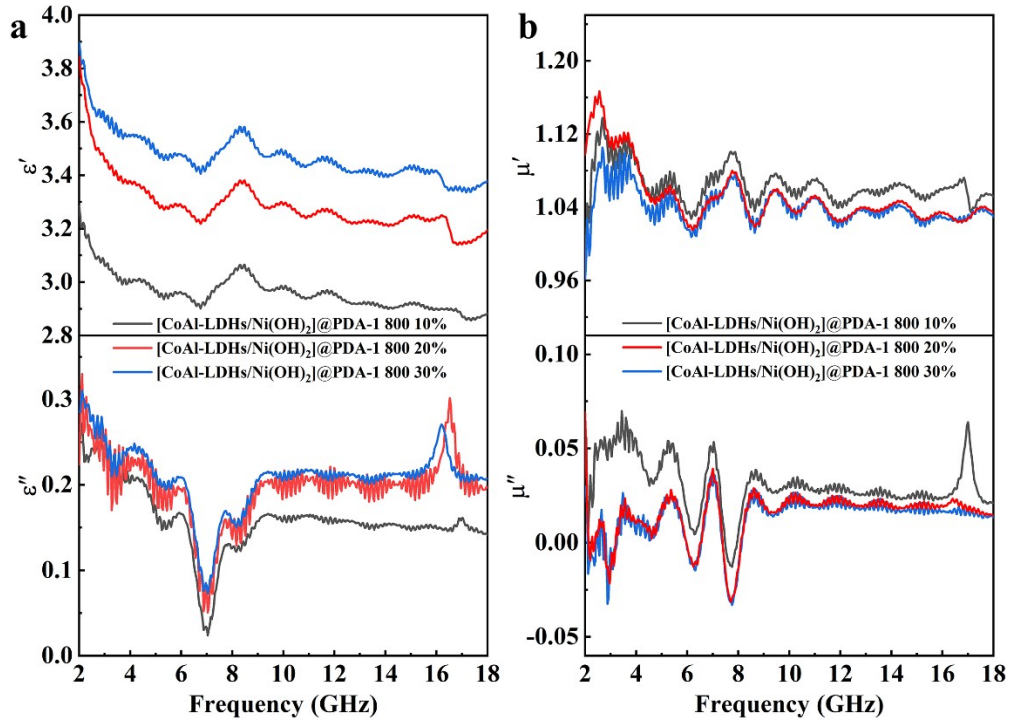


**Fig. S8.** (a) complex permittivity, and (b) complex permeability of [CoAl-LDHs/Ni(OH)<sub>2</sub>]@PDA-1.

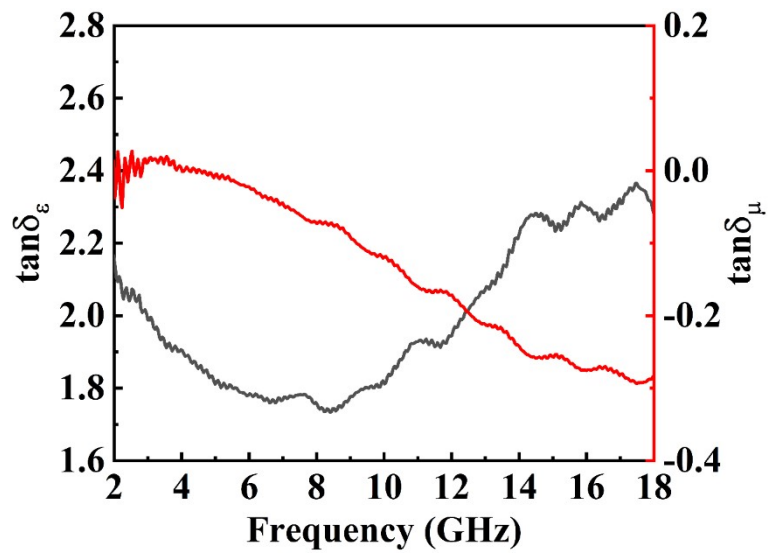


**Fig. S9.** Dielectric loss tangent and magnetic loss tangent curves of CNC-3.

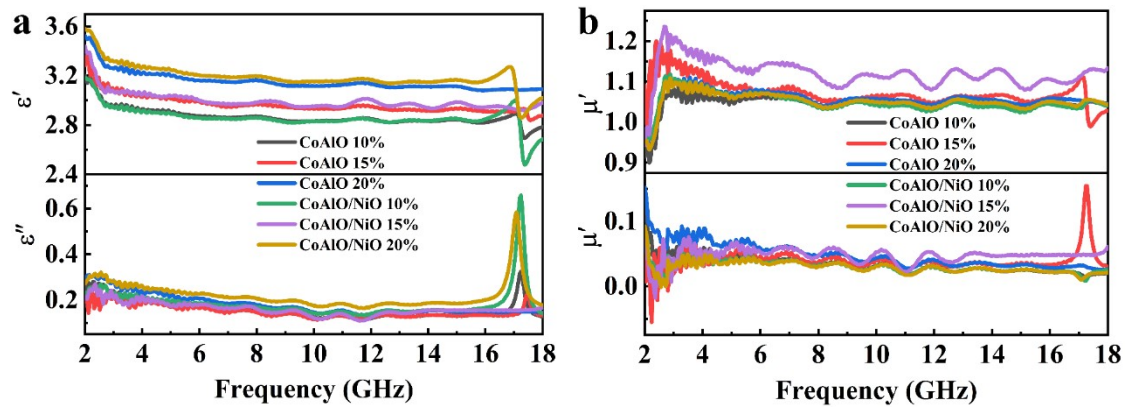


**Fig. S10.** (a) complex permittivity, (b) complex permeability of CoAlO and CoAlO/NiO.

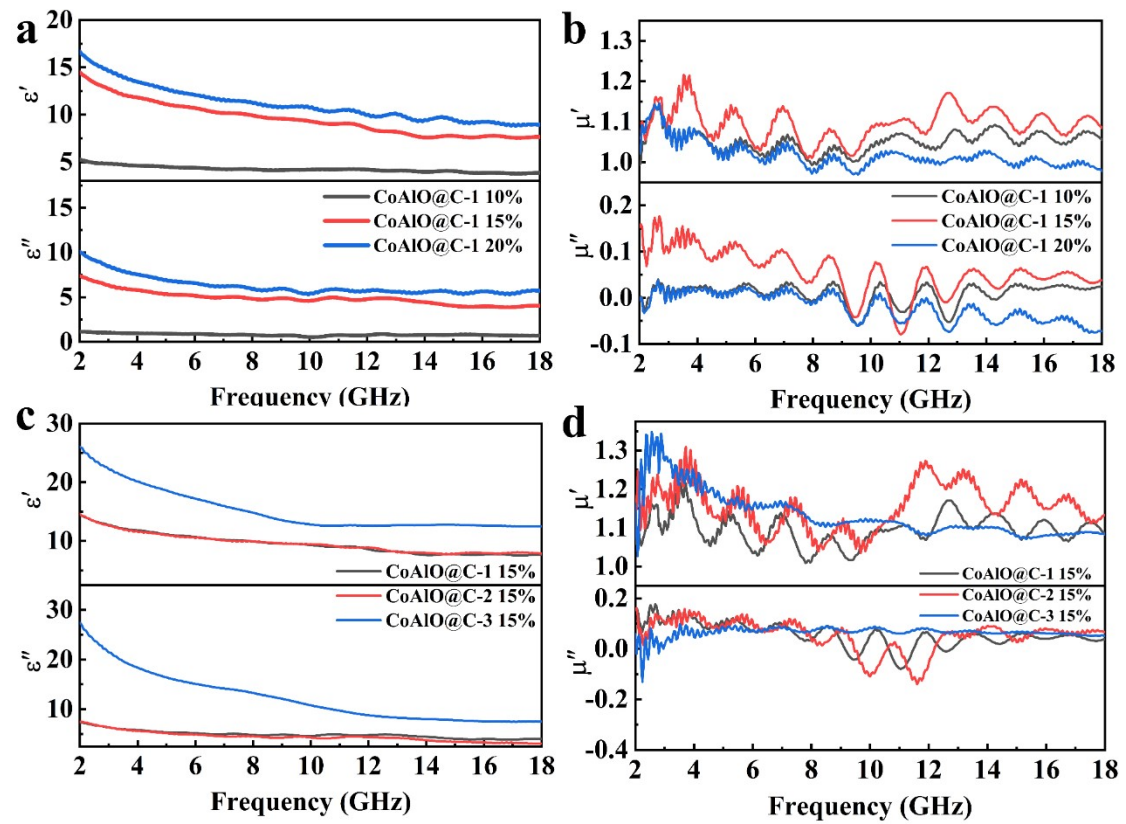


**Fig. S11.** (a, c) complex permittivity and (b, d) complex permeability of CoAlO@C.

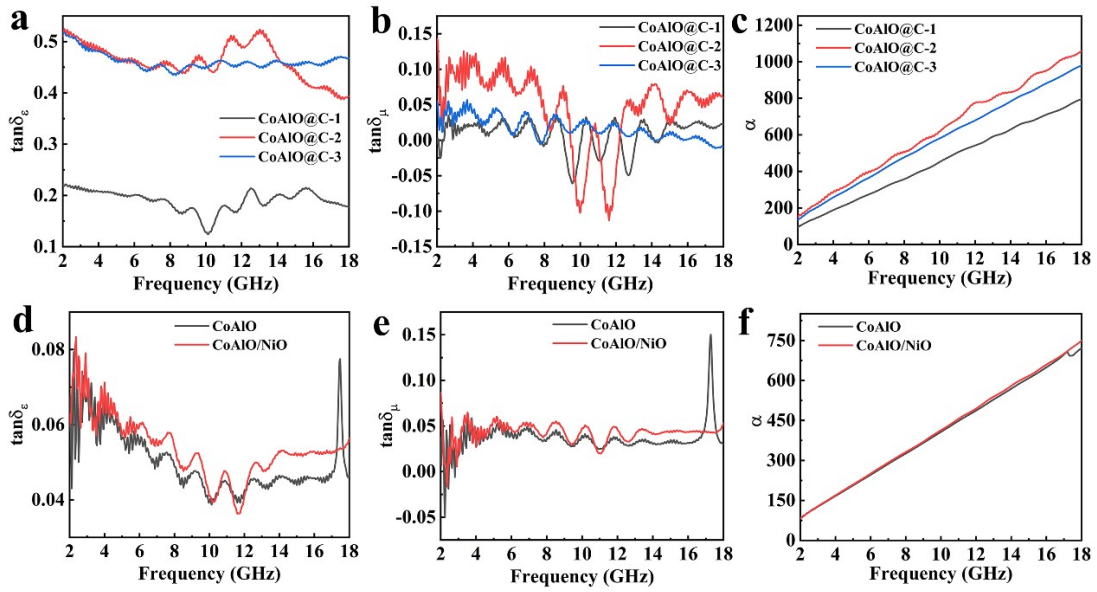


**Fig. S12.** (a, d) Dielectric loss tangent, (b, e) magnetic loss tangent, (c, f)  $\alpha$  curves of CoAlO@C, CoAlO and CoAlO/NiO with filler content of 15 wt%.

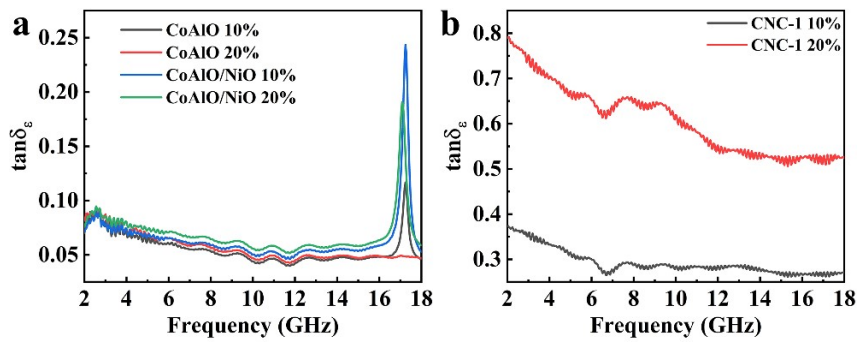


**Fig. S13.** Dielectric loss tangent of (a) CoAlO and CoAlO/NiO, (b) CNC at different filling amount.

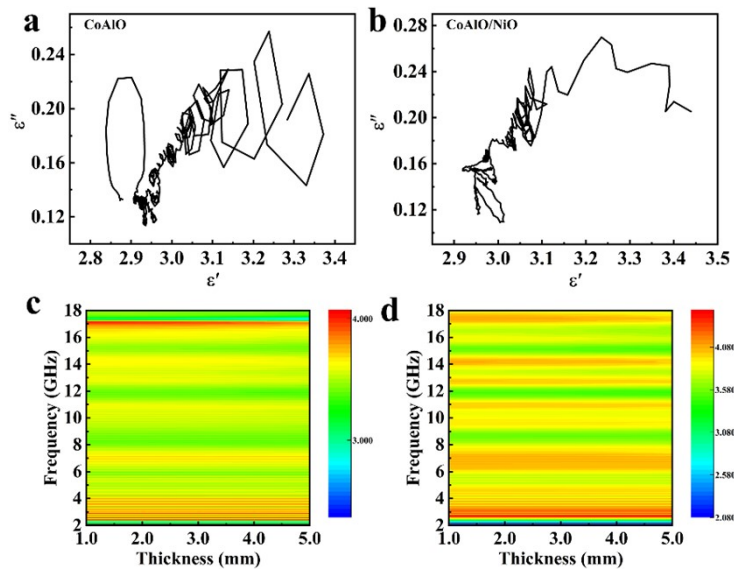


**Fig. S14.** (a-b) Cole-Cole plots, (c-d) impedance matching of CoAlO and CoAlO/NiO.

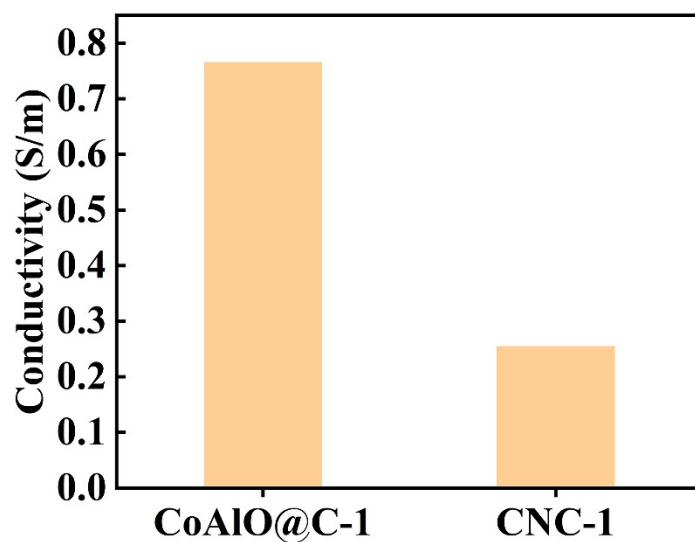


Fig. S15. Electrical conductivity values of CoAlO@C-1 and CNC-1 mixed with PVDF.

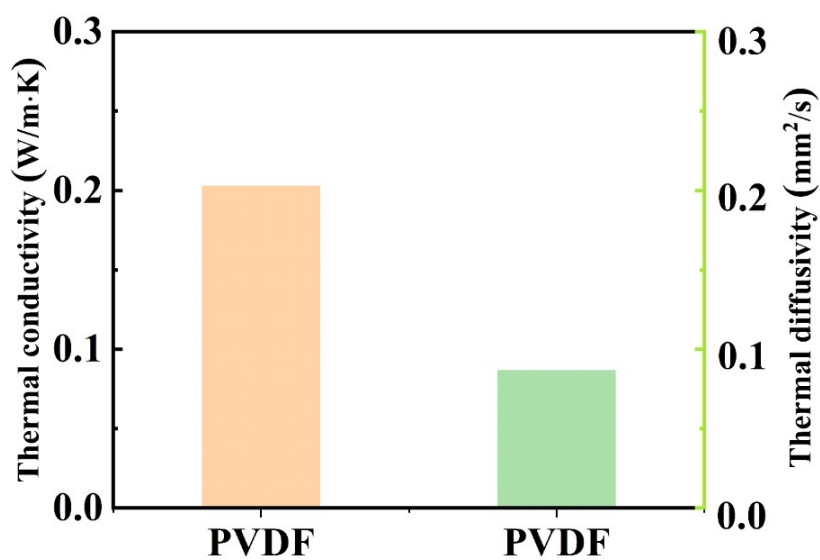


Fig. S16. thermal conductivity and thermal diffusivity of PVDF.

## References

- [1] B. Cai, L. Zhou, P. Zhao, H. Peng, Z. Hou, P. Hu, L. Liu and G. Wang, *Nat. Commun.*, 2024, **15**, 3299.
- [2] L. Liang, X. Yang, C. Li, R. Yu, B. Zhang, Y. Yang and G. Ji, *Adv. Mater.*, 2024, **36**, 2313939.
- [3] S. Hui, X. Zhou, L. Zhang and H. Wu, *Adv. Sci.*, 2024, **11**, 2307649.
- [4] M. Ahmad, M.R. Tariq, A. Menier Al, I. Khan and B. Zhang, *Compos. Pt. A-Appl. Sci. Manuf.*, 2024, **187**, 108445.
- [5] N. Wang, Y. Chen, H. Rao, Y. Zou, K. Nan and Y. Wang, *Carbon*, 2025, **232**, 119824.
- [6] Y. Deng, M. Yang, Y. Wang, M. Wang, M. Zhang, S. Zhou, X. Lu, X. Jian and Y. Chen, *J. Mater. Chem. A*, 2024, **12**, 32172.
- [7] C. Liu, N. Wu, F. Pan, X. Zhang, Z. Wang, L. Wu, J. Lin, W. Liu, J. Liu and Z. Zeng, *Compos. Pt. B-Eng.*, 2024, **287**, 111835.